

High-field spectroscopy of singlet-triplet transitions in the spin-dimer systems $\text{Sr}_3\text{Cr}_2\text{O}_8$ and $\text{Ba}_3\text{Cr}_2\text{O}_8$

Zhe Wang,¹ D. Kamenskyi,^{2,*} O. Cépas,³ M. Schmidt,¹ D. L. Quintero-Castro,⁴ A. T. M. N. Islam,⁴ B. Lake,^{4,5} A. A. Aczel,^{6,7} H. A. Dabkowska,⁸ A. B. Dabkowski,⁸ G. M. Luke,⁶ Yuan Wan,⁹ A. Loidl,¹ M. Ozerov,² J. Wosnitzer,^{2,10} S. A. Zvyagin,² and J. Deisenhofer¹

¹*Experimental Physics V, Center for Electronic Correlations and Magnetism, Institute of Physics, University of Augsburg, 86135 Augsburg, Germany*

²*Dresden High Magnetic Field Laboratory (HLD),*

Helmholtz-Zentrum Dresden-Rossendorf, 01328 Dresden, Germany

³*Institut Néel, CNRS and Université Joseph Fourier, BP 166, 38042 Grenoble Cedex 9, France*

⁴*Helmholtz-Zentrum Berlin für Materialien und Energie, 14109 Berlin, Germany*

⁵*Institut für Festkörperphysik, Technische Universität Berlin, 10623 Berlin, Germany*

⁶*Department of Physics and Astronomy, McMaster University, Hamilton, Ontario L8S 4M1, Canada*

⁷*Quantum Condensed Matter Division, Oak Ridge National Laboratory, Oak Ridge, TN 37831, USA*

⁸*Brockhouse Institute for Materials Research, McMaster University, Hamilton, Ontario L8S 4M1, Canada*

⁹*Department of Physics and Astronomy, Johns Hopkins University, Baltimore, Maryland 21218, USA*

¹⁰*Institut für Festkörperphysik, Technische Universität Dresden, 01068 Dresden, Germany*

(Dated: February 11, 2014)

Magnetic excitations in the isostructural spin-dimer systems $\text{Sr}_3\text{Cr}_2\text{O}_8$ and $\text{Ba}_3\text{Cr}_2\text{O}_8$ are probed by means of high-field electron spin resonance at sub-terahertz frequencies. Three types of magnetic modes were observed. One mode is gapless and corresponds to transitions within excited states, while two other sets of modes are gapped and correspond to transitions from the ground to the first excited states. The selection rules of the gapped modes are analyzed in terms of a dynamical Dzyaloshinskii-Moriya interaction, suggesting the presence of phonon-assisted effects in the low-temperature spin dynamics of $\text{Sr}_3\text{Cr}_2\text{O}_8$ and $\text{Ba}_3\text{Cr}_2\text{O}_8$.

PACS numbers: 78.30.-j, 76.30.-v, 78.20.-e

I. INTRODUCTION

High-field electron spin resonance (ESR) is a very powerful mean to study the excitation spectrum and the transition matrix elements resulting from the coupling between radiation and matter. In magnetic systems, the transitions do not always result from the Zeeman coupling of the spins to the magnetic field of the radiation but may result from indirect processes,^{1,2} thus providing information on these couplings.

Magnetic systems consisting of a small number of interacting magnetic moments in a cluster are particularly interesting in this respect. The simplest cluster is a spin dimer of two spin-1/2 ions coupled by an antiferromagnetic Heisenberg interaction $J_0 > 0$, leading to a singlet ground state ($S = 0$) separated from a triplet excitation ($S = 1$) by an energy gap. In general, because the dimers are regularly arranged in a crystal and coupled to their neighbours, the triplet excitations acquire a dispersion. However, the overall simple picture of the excitation spectrum may remain the same if the interactions are weak or frustrated.

Singlet-triplet transitions have been observed by inelastic neutron scattering and high-field ESR measurements in many spin-dimer antiferromagnets, e.g., $\text{SrCu}_2(\text{BO}_3)_2$ ^{3,4} and CuTe_2O_5 ⁵ based on Cu^{2+} ($3d^9$, $s = 1/2$) ions, and $\text{Ba}_3\text{Cr}_2\text{O}_8$ ⁶⁻⁸ and $\text{Sr}_3\text{Cr}_2\text{O}_8$ ⁹⁻¹¹ based on Cr^{5+} ($3d^1$, $s = 1/2$) ions. While the dispersion as a function of wavevector and energy can be measured,

for example, by single crystal inelastic neutron scattering, photons of the relevant energy usually probe only the Γ point. Moreover, such direct singlet-triplet transitions with $\Delta S = 1$ (magnon-like) are optically forbidden. Their observation implies that the total spin S is not a good quantum number, i.e., rotation symmetry in spin-space is broken. This naturally arises when spin-orbit coupling is present, but the effects are weak for $3d$ transition metal ions.

A first possibility is to consider the small static spin-orbit corrections to the Heisenberg coupling (spin anisotropies), the largest of them in $s = 1/2$ systems being the Dzyaloshinskii-Moriya coupling. Such an interaction was suggested to explain the origin of the observed transitions in $\text{Ba}_3\text{Cr}_2\text{O}_8$ on the condition of a putative lower crystal symmetry,⁷ lower than the observed one. The crystal structure of $\text{Sr}_3\text{Cr}_2\text{O}_8$ and $\text{Ba}_3\text{Cr}_2\text{O}_8$ is hexagonal at room temperature with space group $R\bar{3}m$.^{12,13} Each Cr^{5+} ion with a single $3d$ electron is surrounded by an oxygen tetrahedron. The Jahn-Teller distortion leads to a structural phase transition to a low-temperature monoclinic structure with space group $C2/c$, see Fig. 1(a).^{6,14,15} Two adjacent CrO_4 tetrahedra along the hexagonal c_h direction form a spin dimer with an inversion center [Fig. 1(a)(d)].^{14,16,17}

Here we investigate the singlet-triplet transitions both in $\text{Sr}_3\text{Cr}_2\text{O}_8$ and $\text{Ba}_3\text{Cr}_2\text{O}_8$ by measuring high-field ESR transmission spectra with different radiation polarizations and external magnetic field orientations. We ar-

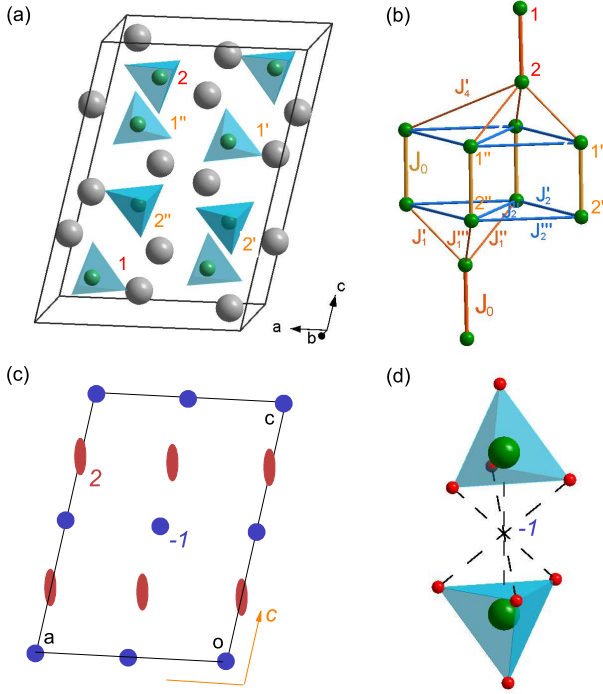


FIG. 1: (Color online) (a) Unit cell of $A_3\text{Cr}_2\text{O}_8$ ($A = \text{Sr}, \text{Ba}$) in the low-temperature monoclinic phase with space group $C2/c$. (b) Layered structure of spin dimers with anisotropic exchange interactions from Ref. 9. J_0 is the intra-dimer exchange interaction. Cr pairs are labeled by (12), (1'2') and (1''2'') in accord with (a). (c) Symmetry elements of the space group $C2/c$: inversion center -1 , two-fold rotation 2 , and glide plane c with glide vector $(0,0,1/2)$ marked in the crystalline ac -plane.²⁸ (d) The Cr^{5+} ($s = 1/2$) spin dimer composed of two CrO_4 tetrahedra with local inversion center -1 . Green, red, and gray spheres denote Cr, O, and Sr/Ba ions, respectively.

gauge that these transitions may occur in the absence of an assumed static symmetry breaking,⁷ provided that the Dzyaloshinskii-Moriya interaction is *dynamical*, *i.e.*, that dynamical lattice distortions break the symmetry instantaneously. In this case, the transitions would result from exciting the electric dipoles formed by the ions of the spin dimers by the electric field of the radiation. Such electric field induced transitions have appeared in different contexts, *e.g.*, as an explanation of *umklapp* $q \approx \pi$ transitions,¹⁸ magnon-like forbidden transitions in spin-gapped systems,^{4,19,20} or electromagnon excitations in multiferroic compounds.²¹ In these latter works, the coupling to the phonons plays an important role and can directly contribute to spin relaxation process.²² An explicit proof of the electric vs. magnetic dipole character is not always possible, but was given in $\text{SrCu}_2(\text{BO}_3)_2$.⁴

II. EXPERIMENTAL DETAILS

High-quality single crystals of $\text{Sr}_3\text{Cr}_2\text{O}_8$ and $\text{Ba}_3\text{Cr}_2\text{O}_8$ were grown by the floating-zone method as described in Refs. 16 and 17, and characterized in detail.^{9–11,23–26} At the Dresden High Magnetic Field Laboratory, a tunable-frequency ESR spectrometer equipped with a 16 T superconducting magnet is employed (similar to that described in Ref. 27). Backward Wave Oscillators (BWOs) and VDI microwave sources (product of Virginia Diodes Inc.) were used as tunable sources of mm- and sub-mm wavelength radiation. Polarized ESR experiments were performed in Voigt geometry with home-made grid polarizers glued directly on the sample. For the Voigt geometry the propagating vector of the electromagnetic wave is aligned perpendicular to the external magnetic field. High-field transmission experiments in Augsburg were performed in Voigt geometry with BWOs covering frequencies from 115 GHz to 1.4 THz and a magneto-optical cryostat (Oxford Instruments/Spectromag) with applied magnetic fields up to 7 T. Single crystals of $\text{Ba}_3\text{Cr}_2\text{O}_8$ and $\text{Sr}_3\text{Cr}_2\text{O}_8$ with typical sizes $4 \times 2 \times 0.2 - 1 \text{ mm}^3$ were measured in the high-field ESR experiments. The crystals are aligned with respect to the hexagonal axes a_h , b_h , and c_h . In the following, the monoclinic axes are noted as a , b and c .

III. EXPERIMENTAL RESULTS AND DISCUSSION

A. Spin triplet excitations

The spin dimers form a layered structure stacked in an $ABAB$ sequence in the low-temperature phase [Fig. 1(a)(b)]. The intra-dimer exchange interaction J_0 (5.5 meV in $\text{Sr}_3\text{Cr}_2\text{O}_8$ and 2.4 meV in $\text{Ba}_3\text{Cr}_2\text{O}_8$) is larger than the inter-dimer interactions.^{6,9} Due to the double-layer structure, the triplet excitations have two branches, *i.e.*, an acoustic mode ω^+ and an optical mode ω^- , corresponding to the “ $q = 0$ ” and “ $q = \pi$ ” phase difference between spin dimers of adjacent layers, respectively.^{29,30} The excitation energies at the zone center are given by a random phase approximation calculation^{6,9}

$$\omega^\pm = \sqrt{J_0^2 + J_0\gamma^\pm} \quad (1)$$

where $\gamma^\pm = 2(J_2' + J_2'' + J_2''') \pm [(J_1' + J_1'' + J_1''') + (J_4' + J_4'' + J_4''')]$. The different exchange constants J_i denote intra- and inter-layer interactions as illustrated in Fig. 1(b) and were extracted from inelastic neutron scattering.^{6,9} Both modes are triplets and split in an external magnetic field with energies $\omega^\pm(H) = \omega^\pm + g\mu_B H S^z$ with $S^z = 0, \pm 1$ [Fig. 2(a)]. This picture is confirmed by unpolarized transmission ESR measurements up to 16 T for $\text{Sr}_3\text{Cr}_2\text{O}_8$ and 13 T for $\text{Ba}_3\text{Cr}_2\text{O}_8$ as shown in Fig. 2(b)

and Fig. 3(a), respectively. Note that excitations to the $S^z = 0$ levels are absent because of the sweeping field technique. The obtained excitation energies extrapolated to zero field are $\omega^+ = 1.47$ THz (6.1 meV) and $\omega^- = 1.24$ THz (5.1 meV) for $\text{Sr}_3\text{Cr}_2\text{O}_8$, and $\omega^+ = 563$ GHz (2.3 meV) and $\omega^- = 399$ GHz (1.6 meV) for $\text{Ba}_3\text{Cr}_2\text{O}_8$ with $g = 1.94(3)$ for both compounds. The energies are perfectly consistent with inelastic neutron experiments,^{6,9} which also measured their triplet nature.⁶ The acoustic mode has higher energy than the optical mode in both compounds because the inter-dimer couplings are dominated by antiferromagnetic exchange interactions.^{6,9} In the extrapolation, there is no zero field splitting of the different S^z components detectable within the experimental uncertainty.

B. Polarization analysis

ESR transmission experiments were performed for different directions of the polarization of the electromagnetic radiation and orientations of the external magnetic field with respect to the hexagonal axes of $\text{Sr}_3\text{Cr}_2\text{O}_8$ and $\text{Ba}_3\text{Cr}_2\text{O}_8$ (Figs. 2,3). The field-dependence of the singlet-triplet excitations has been determined in the unpolarized experiments [Fig. 2(b) and Fig. 3(a)]. One can accordingly identify the excitations in the spectra measured with polarized radiations.

Figures 2(c)-(f) show polarized ESR transmission spectra of $\text{Sr}_3\text{Cr}_2\text{O}_8$ measured with respect to the hexagonal axes. The acoustic mode 1 and the optical mode 3' are observed and are in agreement with the unpolarized spectra shown in Fig. 2(b). In a finite external magnetic field, the acoustic modes and optical modes exhibit different polarization dependencies: the acoustic modes are observed for all the polarizations, while the optical modes are absent for $E^\omega \parallel c_h, H \parallel c_h$ [Fig. 2(f)].

Figure 3(b)-(d) shows the polarized ESR transmission spectra of $\text{Ba}_3\text{Cr}_2\text{O}_8$ with various polarization configurations. One can identify the acoustic mode 1, the optical modes 1',3', and the intra-triplet mode 2 in accord with Fig. 3(a). The most prominent feature is also that the optical modes are absent only for $E^\omega \parallel c_h, H \parallel c_h$, while the acoustic modes are observed for all the polarizations in $\text{Ba}_3\text{Cr}_2\text{O}_8$.

Considering the geometric relations $c_h = (a + 3c)/2$,³¹ $b_h = (-a + b)/2$, $a_h = (a + b)/2$ between hexagonal and monoclinic axes,⁹ the contribution of the monoclinic axes a and b are probed simultaneously in the polarization measurements for $E^\omega \parallel b_h$ and for $E^\omega \parallel a_h$. Thus, $\text{Sr}_3\text{Cr}_2\text{O}_8$ and $\text{Ba}_3\text{Cr}_2\text{O}_8$ exhibit the same polarization dependent selection rules, which are summarized in Table I.

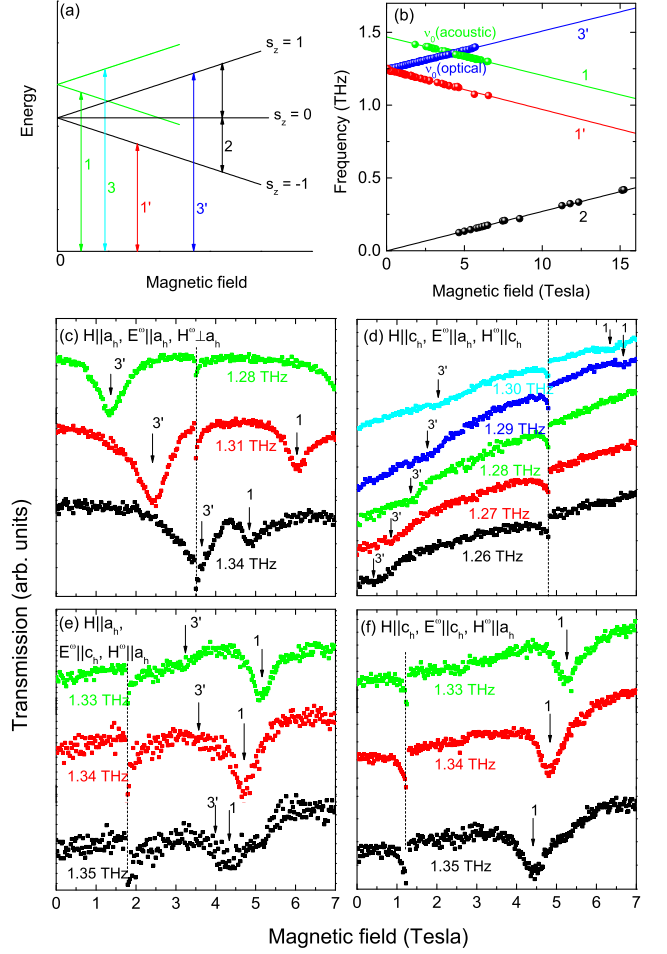


FIG. 2: (Color online) $\text{Sr}_3\text{Cr}_2\text{O}_8$ (a) Schematic singlet-triplet excitations in an external magnetic field. 1 and 3 are the acoustic modes, and 1' and 3' are the optical modes. The two types of modes originate from the two inequivalent layers in the unit cell. Mode 2 denotes the intra-triplet excitations. The singlet-triplet excitations are measured with no polarization analysis (b) and with polarization analysis (E^ω, H^ω) (c)-(f) for different orientations of applied magnetic field H at 2 K. The vertical dashed lines indicate artifacts due to spark lines from the BWOs.

C. Discussion

A magnetic dipole singlet-triplet excitation in a single dimer can be observed when there is an intra-dimer static Dzyaloshinskii-Moriya interaction. Since this is forbidden in $\text{Sr}_3\text{Cr}_2\text{O}_8$ and $\text{Ba}_3\text{Cr}_2\text{O}_8$ due to the inversion center in the middle of the bonds in the Cr_2O_8 dimers [Fig. 1(d)], the observed transitions have been ascribed to additional undetected lattice distortions that break the inversion symmetry.⁷ However, other mechanisms may be at play which do not need to invoke additional distortions.

One can keep the magnetic dipole mechanism in a pure magnetic model and consider the weaker dimer-dimer in-

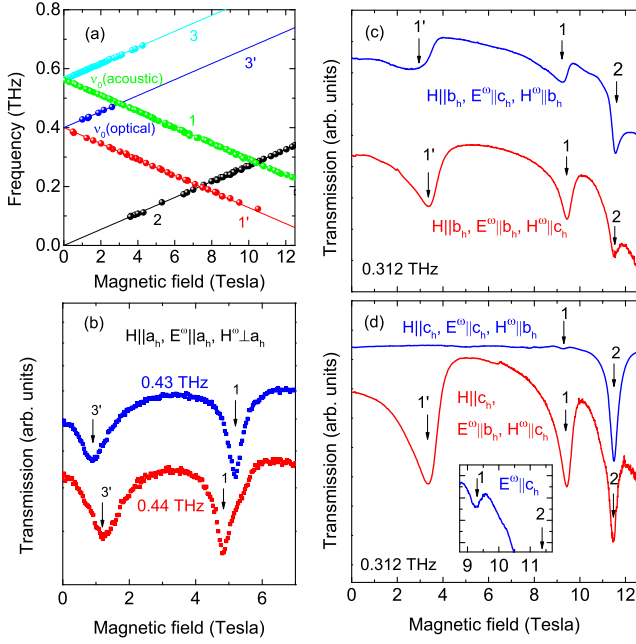


FIG. 3: (Color online) $\text{Ba}_3\text{Cr}_2\text{O}_8$ (a) Singlet-triplet excitations. Polarized transmission spectra measured at 2 K (b) and at 1.4 K (c,d). In (c), H^ω is parallel to the $a_h b_h$ -plane. Inset: enlarged view of the spectrum for $H||c_h$, $E^\omega||c_h$, and $H^\omega||b_h$.

TABLE I: Experimentally observed spin singlet-triplet excitations in the polarized ESR spectra in the *hexagonal* notations. The acoustic mode 1 and optical mode 1', 3' are noted as '0' and 'π', respectively, for short.

$E^\omega \backslash H$	a_h	b_h	c_h
a_h	$0 + \pi$ [Fig. 2(c), 3(b)]		$0 + \pi$ [Fig. 2(d)]
b_h		$0 + \pi$ [Fig. 3(c)]	$0 + \pi$ [Fig. 3(d)]
c_h	$0 + \pi$ [Fig. 2(e)]	$0 + \pi$ [Fig. 3(c)]	0 [Fig. 2(f), 3(d)]

interactions. Static inter-dimer Dzyaloshinskii-Moriya interactions along the superexchange paths of J_1 , J_2 , and J_4 (but not J_3 which has an inversion center) can mix the singlet and triplet states, and allow the magnetic dipole transitions.³² However, we consider it more likely that an electric dipole mechanism involving the strongest exchange interactions dominates the excitation intensities. This is because (1) a static singlet-triplet mixing generally bends the magnetization curves (this is not observed in the present compounds^{7,24}) and opens a zero-field splitting (which is not detectable here and less than a few GHz); and (2) rough estimates of relative intensities tend to favor the electric dipole mechanism,²⁰ *a fortiori* when the magnetic dipole transitions are plagued by an additional small parameter, $\sim J'/J_0$.

We consider an electric-dipole coupling between radiation and spins,

$$W = \sum_{i,\alpha,\beta} E_\alpha^\omega A_{\alpha\beta} (\mathbf{S}_{i1} \times \mathbf{S}_{i2})_\beta \quad (2)$$

where i refers to the spin dimers, and $A_{\alpha\beta}$ is a coupling constant that couples the electric field of the radiation along the α direction with the vector product of spins along the β direction, that has the Dzyaloshinskii-Moriya symmetry. This is the simplest spin operator for $s = 1/2$ systems that breaks spin rotation symmetry (but not the time-reversal symmetry), and allows for a non-zero matrix element for singlet-triplet transitions.

Operators of the same form have been used to explain double magnon excitations in several antiferromagnetic systems,^{33,34} and similar processes in dimer systems,^{19,20} but the microscopic mechanism remains unclear. In the latter case, it is assumed that an *optical* phonon breaks the inversion symmetry within the dimer instantaneously. Since the electronic hopping is much faster than lattice vibrations, superexchange takes place in a dimer with no inversion center. The Dzyaloshinskii-Moriya interaction is therefore generated thanks to the spin-orbit coupling, and is linear in the ionic displacements at first order. Typically $A_{\alpha\beta} = D^\alpha d^\beta$ where d^β is the instantaneous Dzyaloshinskii-Moriya vector and D^α the electric dipole of the unit cell created by the virtual phonon (see an example in Fig. 4).

Symmetry arguments. The coupling constant $A_{\alpha\beta}$ must be constrained by the crystal symmetries of the lattice in the presence of the radiation electric field. In particular, they should be identical from unit cell to unit cell but may vary within the unit cell. The space group $C2/c$ has four symmetry elements, namely, identity 1 , inversion center -1 , two-fold rotation axis 2 , and ac -glide plane c with glide vector $(0, 0, 1/2)$, as shown in Fig. 1(c).²⁸ The last two symmetry operations always transform the pseudo-vector $\mathbf{T}_{12} \equiv \mathbf{S}_1 \times \mathbf{S}_2$ of the two dimerized spins in one layer onto one in the next layer, labeled with primes, as in Fig. 1(b). By using these symmetries, we constrain the coupling constants:

- $E^\omega||a, c$: the ac glide plane leaves E^ω invariant, transforms T_{12}^b onto $T_{1'2'}^b$, and $T_{12}^{a,c}$ onto $-T_{1'2'}^{a,c}$ (Fig. 1). The coupling constants $A_{\alpha\beta}$ within the unit cell are therefore not independent but only the \pm phases appear: the operator W in Eq. (2) will generate excitations to the acoustic and optical branches, respectively.
- $E^\omega||b$: the two-fold rotation axis is along the b axis. It leaves E^ω invariant and transforms T_{12}^b onto $-T_{1'2'}^b$, and $T_{12}^{a,c}$ onto $T_{1'2'}^{a,c}$: the operator W will generate excitations to the optical and acoustic branches, respectively.

Based on the symmetries, this mechanism predicts the transitions to occur at the energies of the acoustic and optical modes, in perfect agreement with the energies

observed for both compounds. We emphasize that no static breaking of inversion symmetry is needed.

A finite external magnetic field \mathbf{H} splits the triplet modes and each mode has its own intensity. If all the involved pseudo-vectors \mathbf{T}_{ij} in the operator W are parallel to the magnetic field $\mathbf{H} \parallel z$, only the transition to the $S^z = 0$ component of the triplet occurs, but it is invisible in the present high-field ESR setup. Therefore only the components of \mathbf{T}_{ij} that are perpendicular to \mathbf{H} generate observable transitions. Taking into account the symmetry arguments given above, we infer the results given in Table II.

TABLE II: *Theoretically* predicted excitations to the $S^z = \pm 1$ triplet components according to the dynamical mechanism in the *monoclinic* notations. The acoustic mode and optical mode are noted here as '0' and ' π ', respectively, for short. The responsible matrix elements are given in the brackets following the corresponding modes.

$E^\omega \backslash H$	a	b	c
a	$0(A_{ab}) + \pi(A_{ac})$	$\pi(A_{aa}, A_{ac})$	$0(A_{ab}) + \pi(A_{aa})$
b	$0(A_{bc}) + \pi(A_{bb})$	$0(A_{ba}, A_{bc})$	$0(A_{ba}) + \pi(A_{bb})$
c	$0(A_{cb}) + \pi(A_{cc})$	$\pi(A_{ca}, A_{cc})$	$0(A_{cb}) + \pi(A_{ca})$

We cannot strictly test experimentally the selection rules given in Table II, because in the low-temperature phase the samples have three monoclinic twins rotated about the c_h axis by an angle of 60° with each other.⁹ As a consequence, a field applied along the hexagonal axis, a_h or b_h , has components along a and b , thus mixing the selection rules. Furthermore, the hexagonal c_h -axis is tilted from the c -axis by 12° , so that a field applied along c_h has a main component along c but also a small component along a . The mixing of the different components implies that both modes are predicted to have finite intensities in all the experimental configurations studied here, if the corresponding couplings $A_{\alpha\beta}$ (given in Table II) are non-zero. However, the optical mode is not detected in the configuration $E^\omega \parallel c_h$, $H \parallel c_h$, see Table I. If we ignore the difference between the c_h and c axes (which is small), the extinction of the optical mode for the configuration $E^\omega \parallel c_h$, $H \parallel c_h$ can be interpreted by postulating a vanishing (or weak) coupling constant $A_{ca} = 0$, see Table II. Given that all the coupling elements are allowed by symmetry in the low temperature phase, it is difficult to prove that A_{ca} vanishes.

We now discuss this extinction as the result of a possible approximate symmetry, originating from the higher symmetry of the high-temperature phase. In the high-temperature phase, there are three mirror planes at 120° bisecting the basal O-O bonds and containing the two Cr ions of the dimer. Since E^ω along c_h does not break these symmetries, the instantaneous Dzyaloshinskii-Moriya vector should be perpendicular to all, and hence would vanish. None of these mir-

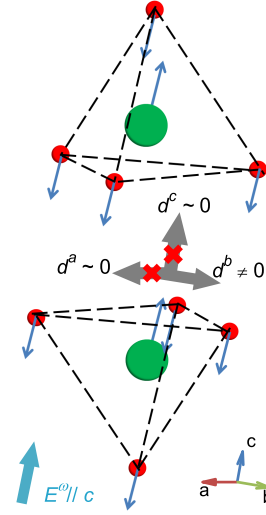


FIG. 4: (Color online) Illustration of the coupling constants $A_{ca} \sim 0$, $A_{cb} \neq 0$, and $A_{cc} \sim 0$. The spin dimer Cr_2O_8 distorts in the radiation electric field $E^\omega \parallel c$ with associated instantaneous Dzyaloshinskii-Moriya vectors d^a , d^b , and d^c .

ror planes are exact symmetries in the low-temperature phase, but one of them coincides with the ac plane and contains the two Cr ions.^{14,28} If we assume that this plane remains an approximate mirror plane, the instantaneous Dzyaloshinskii-Moriya vector would be along the b axis, when $E^\omega \parallel a, c$ respects this symmetry, *i.e.*, $A_{ab} \neq 0$, $A_{cb} \neq 0$. Therefore we would expect zero couplings ($A_{aa} = 0$, $A_{ac} = 0$, $A_{ca} = 0$, $A_{cc} = 0$) if this symmetry were exactly preserved, or approximately zero if this symmetry were weakly broken. This gives a justification for the extinction of the optical mode in both compounds ($A_{ca} \approx 0$). It is also consistent with the weak intensity of the optical mode for the configuration $E^\omega \parallel c_h$, $H \parallel a_h$ which is observed in $\text{Sr}_3\text{Cr}_2\text{O}_8$ [Fig. 2(e)], provided that $A_{cc} \approx 0$ is weak. However, in $\text{Ba}_3\text{Cr}_2\text{O}_8$ with the configuration $E^\omega \parallel c_h$, $H \parallel b_h$ [Fig. 3(c)] the optical mode is much stronger. Within the present mechanism, this can be interpreted only with a finite $A_{cc} \neq 0$ (since $A_{ca} \approx 0$). This possibly implies that the symmetry discussed is more strongly broken in the low temperature phase in $\text{Ba}_3\text{Cr}_2\text{O}_8$ than in $\text{Sr}_3\text{Cr}_2\text{O}_8$.

Other mechanisms cannot be completely discarded by the present study, especially because it is difficult to assess their relative intensities. The present one, however, gives a consistent interpretation of the experimental results and would remain operative in systems with arbitrarily weak coupling between dimers with an inversion center.

IV. CONCLUSIONS

By performing polarization-dependent high-field spectroscopy measurements at low temperature, we have

found that the three-dimensional spin dimerized anti-ferromagnets $\text{Ba}_3\text{Cr}_2\text{O}_8$ and $\text{Sr}_3\text{Cr}_2\text{O}_8$ exhibit the same polarization dependence of spin singlet-triplet excitations, thus confirming the same spin symmetry in both compounds. Restricting to the isolated dimer picture, we have explored an electric dipole active mechanism that provides an explanation for the occurrence of both the acoustic and optical modes. In this mechanism, the previously assumed but symmetry-forbidden static Dzyaloshinskii-Moriya coupling is replaced by instantaneous couplings to the phonons. From the observed selection rules, some of these couplings are inferred to vanish (or to be weak), suggesting that the lattice symmetry

that we have identified may in fact be only weakly broken across the structural phase transition.

Acknowledgments

We thank V. Tsurkan for help with sample preparation. We acknowledge partial support by the Deutsche Forschungsgemeinschaft via TRR 80 (Augsburg-Munich), Project DE 1762/2-1 and ZV 6/2-1, and also the support of the HLD at HZDR, member of the European Magnetic Field Laboratory.

-
- * Present address: Radboud University Nijmegen, Institute for Molecules and Materials, High Field Magnet Laboratory, 6500 GL Nijmegen, The Netherlands.
- ¹ R. J. Elliott and R. Loudon, Phys. Lett. **3**, 189 (1963).
 - ² Y. R. Shen and N. Bloembergen, Phys. Rev. **143**, 372 (1966).
 - ³ H. Nojiri, H. Kageyama, K. Onizuka, Y. Ueda, and M. Motokawa, J. Phys. Soc. Jpn. **68**, 2906 (1999).
 - ⁴ T. R  m, D. H  vonen, U. Nagel, Y.-J. Wang, T. Timusk, and H. Kageyama, Phys. Rev. B **70**, 144417 (2004).
 - ⁵ Z. Wang, M. Schmidt, Y. Goncharov, Y. Skourski, J. Wosnitza, H. Berger, H.-A. Krug von Nidda, A. Loidl, and J. Deisenhofer, J. Phys. Soc. Jpn. **80**, 124707 (2011).
 - ⁶ M. Kofu, J.-H. Kim, S. Ji, S.-H. Lee, H. Ueda, Y. Qiu, H.-J. Kang, M. A. Green, and Y. Ueda, Phys. Rev. Lett. **102**, 037206 (2009).
 - ⁷ M. Kofu, H. Ueda, H. Nojiri, Y. Oshima, T. Zenmoto, K. C. Rule, S. Gerischer, B. Lake, C. D. Batista, Y. Ueda, and S.-H. Lee, Phys. Rev. Lett. **102**, 177204 (2009).
 - ⁸ D. Kamenskyi, J. Wosnitza, J. Krzystek, A. A. Aczel, H. A. Dabkowska, A. B. Dabkowski, G. M. Luke, and S. A. Zvyagin, J. Low. Temp. Phys. **170**, 231 (2013).
 - ⁹ D. L. Quintero-Castro, B. Lake, E. M. Wheeler, A. T. M. N. Islam, T. Guidi, K. C. Rule, Z. Izaola, M. Russina, K. Kiefer, and Y. Skourski, Phys. Rev. B **81**, 014415 (2010).
 - ¹⁰ Z. Wang, M. Schmidt, A. G  nther, S. Schaille, N. Pascher, F. Mayr, Y. Goncharov, D. L. Quintero-Castro, A. T. M. N. Islam, B. Lake, H.-A. Krug von Nidda, A. Loidl, and J. Deisenhofer, Phys. Rev. B **83**, 201102 (2011); *ibid* **86**, 039901(E) (2012).
 - ¹¹ D. L. Quintero-Castro, B. Lake, A. T. M. N. Islam, E. M. Wheeler, C. Balz, M. M  nsson, K. C. Rule, S. Gvasaliya, and A. Zheludev, Phys. Rev. Lett. **109**, 127206 (2012).
 - ¹² E. Cuno and Hk. M  ller-Buschbaum, Z. Anorg. Allg. Chem. **572**, 95 (1989).
 - ¹³ H. J. Mattausch, and H. K. M  ller-Buschbaum, Z. Naturforsch. B, **27**, 739 (1972).
 - ¹⁴ L. C. Chapon, C. Stock, P. G. Radaelli, and C. Martin, arXiv:0807.0877v2 (2008).
 - ¹⁵ Z. Wang, M. Schmidt, A. G  nther, F. Mayr, Yuan Wan, S.-H. Lee, H. Ueda, Y. Ueda, A. Loidl, and J. Deisenhofer, Phys. Rev. B **85**, 224304 (2012).
 - ¹⁶ A. T. M. Nazmul Islam, D. Quintero-Castro, B. Lake, K. Siemensmeyer, K. Kiefer, Y. Skourski, and T. Herrmannsd  rfer, Crystal Growth & Design **10**, 465 (2010).
 - ¹⁷ A. A. Aczel, H. A. Dabkowska, P. R. Provencher and G. M. Luke, J. Crystal Growth **310**, 870 (2008).
 - ¹⁸ P. P. Mitra and B. I. Halperin, Phys. Rev. Lett. **72**, 912 (1994).
 - ¹⁹ O. C  pas, K. Kakurai, L. P. Regnault, T. Ziman, J. P. Boucher, N. Aso, M. Nishi, H. Kageyama, and Y. Ueda, Phys. Rev. Lett. **87**, 167205 (2001).
 - ²⁰ O. C  pas and T. Ziman, Phys. Rev. B **70**, 024404 (2004).
 - ²¹ A. Pimenov, A. A. Mukhin, V. Yu. Ivanov, V. D. Travkin, A. M. Balbashov and A. Loidl, Nature Phys. **2**, 97 (2006).
 - ²² M. V. Eremin, D. V. Zakharov, H.-A. Krug von Nidda, R. M. Eremina, A. Shuvaev, A. Pimenov, P. Ghigna, J. Deisenhofer, and A. Loidl, Phys. Rev. Lett. **101**, 147601 (2008).
 - ²³ A. A. Aczel, H.A. Dabkowska, J.F. Britten, L.E. Harrington, and G.M. Luke, Acta Crystallographica E **63**, i196 (2007).
 - ²⁴ A. A. Aczel, Y. Kohama, C. Marcenat, F. Weickert, M. Jaime, O. E. Ayala-Valenzuela, R. D. McDonald, S. D. Slesnic, H. A. Dabkowska, and G. M. Luke, Phys. Rev. Lett. **103**, 207203 (2009).
 - ²⁵ A. A. Aczel, Y. Kohama, M. Jaime, K. Ninios, H. B. Chan, L. Balicas, H. A. Dabkowska, and G. M. Luke, Phys. Rev. B **79**, 100409 (2009).
 - ²⁶ D. Wulferding, P. Lemmens, K.-Y. Choi, V. Gnezdilov, J. Deisenhofer, D. Quintero-Castro, A.T.M.N. Islam, and B. Lake, Phys. Rev. B **84**, 064419 (2011).
 - ²⁷ S. A. Zvyagin, J. Krzystek, P.H.M. van Loosdrecht, G. Dhallenne and A. Revcolevschi, Physica B **346-347**, 1 (2004).
 - ²⁸ *International tables for crystallography: Volume A space group symmetry*, edited by Theo Hahn, (Kluwer Academic Publishers, Dordrecht, 1989).
 - ²⁹ B. Leuenberger, A. Stebler, H. U. G  del, A. Furrer, R. Feile, and J. K. Kjems, Phys. Rev. B **30**, 6300 (1984).
 - ³⁰ S. B. Haley and P. Erd  s, Phys. Rev. B **5**, 1106 (1972).
 - ³¹ Instead of the relation $c_h = (-a + 3c)/2$ given in Ref. 14, we choose here the opposite direction as the $+a$ direction in order to be consistent with the crystal structure shown in Fig. 1.
 - ³² T. Sakai, O. C  pas, and T. Ziman, J. Phys. Soc. Jpn. **69**, 3521 (2000).
 - ³³ R. J. Elliott and M. F. Thorpe, J. Phys. C **2**, 1630 (1969).
 - ³⁴ M. Gr  ninger, J. M  nzel, A. Gaymann, A. Zibold, H. P. Geserich, and T. Kopp, Europhys. Lett. **35**, 55 (1996).